Genetics in Medicine

ARTICLE

De novo missense variants in *RRAGC* lead to a fatal mTORopathy of early childhood

Margot R.F. Reijnders[1], Annette Seibt[2], Melanie Brugger[3], Ideke J.C. Lamers[4], Torsten Ott[5], Oliver Klaas[6], Judit Horváth[6], Ailsa M.S. Rose[7], Isabel M. Craghill[7], Theresa Brunet[3,8], Elisabeth Graf[3], Katharina Mayerhanser[3], Debby Hellebrekers[1], David Pauck[9], Eva Neuen-Jacob[9], Richard J.T. Rodenburg[10], Dagmar Wieczorek[11], Dirk Klee[12], Ertan Mayatepek[2], Gertjan Driessen[13], Robert Bindermann[2], Luisa Averdunk[2], Klaus Lohmeier[2], Margje Sinnema[1], Alexander P.A. Stegmann[1], Ronald Roepman[4], James A. Poulter[7], Felix Distelmaier[2,*]

ARTICLE INFO

ABSTRACT

Purpose: Mechanistic target of rapamycin (mTOR) complex 1 (mTORC1) regulates cell growth in response to nutritional status. Central to the mTORC1 function is the Rag-GTPase heterodimer. One component of the Rag heterodimer is RagC (Ras-related GTP-binding protein C), which is encoded by the *RRAGC* gene.

Methods: Genetic testing via trio exome sequencing was applied to identify the underlying disease cause in 3 infants with dilated cardiomyopathy, hepatopathy, and brain abnormalities, including pachygyria, polymicrogyria, and septo-optic dysplasia. Studies in patient-derived skin fibroblasts and in a HEK293 cell model were performed to investigate the cellular consequences.

Results: We identified 3 de novo missense variants in *RRAGC* (NM_022157.4: c.269C>A, p.(Thr90Asn), c.353C>T, p.(Pro118Leu), and c.343T>C, p.(Trp115Arg)), which were previously reported as occurring somatically in follicular lymphoma. Studies of patient-derived fibroblasts carrying the p.(Thr90Asn) variant revealed increased cell size, as well as dysregulation of mTOR-related p70S6K (ribosomal protein S6 kinase 1) and transcription factor EB signaling. Moreover, subcellular localization of mTOR was decoupled from metabolic state. We confirmed the key findings for all *RRAGC* variants described in this study in a HEK293 cell model.

Conclusion: The above results are in line with a constitutive overactivation of the mTORC1 pathway. Our study establishes de novo missense variants in *RRAGC* as cause of an early-onset mTORopathy with unfavorable prognosis.

---

*Correspondence and requests for materials should be addressed to Felix Distelmaier, Department of General Pediatrics, Heinrich-Heine-University, Moorenstr. 5, 40225 Düsseldorf, Germany. *Email address:* felix.distelmaier@med.uni-duesseldorf.de
Affiliations are at the end of the document.

Introduction

RRAG genes encode for Rag proteins that are part of a unique family of small GTPases known to regulate amino acid–induced mechanistic target of rapamycin complex 1 (mTORC1) signaling.[1] All family members, including Ras-related GTP-binding C (RagC), interact with mTORC1 in an amino acid–sensitive manner. For RagC, a GDP-bound state is necessary for amino acid activation of mTORC1 to promote intracellular localization of mTOR to the lysosomal surface, which also contains activator RHEB.[2] RagC additionally mediates phosphorylation of transcription factor EB (TFEB) in a substrate-specific mechanism.[3] Via mTORC1 and TFEB, RagC has an important role in the regulation of key cellular processes, such as autophagy and lysosomal biogenesis, and the regulation of brain developmental aspects, such as neuronal maturation and migration (Supplemental Figure 1 provides an overview).[4,5]

Currently, 2 Rag family members have been associated with human disease: pathogenic variants in *RRAGA* were described in patients with autosomal dominant cataract.[6] *RRAGD* mTOR-activating variants were identified in children with renal tubulopathy and cardiomyopathy.[7] In addition, a variant in *RRAGC* (NM_022157.4:c.224C>A; p.(Ser75Tyr)) has previously been associated with syndromic fetal dilated cardiomyopathy (DCM) in a single individual.[8] The individual died because of intractable multisystem organ failure at the age of 22 months. Further evidence for the pathogenicity of the identified *RRAGC* variant came from functional studies in *RRAGC*^S56Y-mutated AD293 cells and a zebrafish model.[8,9]

Here, we report 3 children with heterozygous de novo missense variants in *RRAGC*. In addition to DCM and hepatopathy, the individuals showed brain anomalies, which included pachygyria, polymicrogyria, and septo-optic dysplasia. Functional studies using patient-derived fibroblasts revealed increased cell size, as well as altered p70S6K and TFEB signaling. Moreover, subcellular localization of mTOR was decoupled from metabolic state. Finally, we confirmed our key findings for all *RRAGC* variants identified in this study using a HEK293 cell model.

Materials and Methods

Genetic testing and identification of additional families

Trio exome sequencing (ES) of individual #1 was performed in a diagnostic setting using DNA extracted from blood as described previously.[10] Sanger sequencing was performed to confirm the variant in blood and fibroblasts. The matchmaking platform GeneMatcher was used to identify additional individuals with overlapping genotype and phenotype.[11] In individuals #2 and #3, trio-ES was performed on DNA extracted from whole blood in a diagnostic setting.

Variants were classified according to the current American College of Medical Genetics and Genomics classification.[12] The study was conducted in accordance with the Declaration of Helsinki. The families agreed to share the medical and genetic information for scientific publication.

Fibroblast culture

Fibroblasts were cultured in Dulbecco's Modified Eagle Medium (DMEM) supplemented with 10% fetal bovine serum (FBS) and 1% penicillin/streptomycin (all from Life Technologies) at 37 °C in a humidified atmosphere of 5% CO_2. For amino acid starvation, we used DMEM without amino acids and glucose powder (US Biological), which was supplemented with 10% dialyzed FBS (Gibco; DMEM – aa). For amino acid supplementation, nonessential amino acids (Gibco), essential amino acids without glutamine (Gibco), and glutamine were added (DMEM + aa). The use of patient-derived cells was approved by the ethical committee of the Heinrich-Heine-University Düsseldorf (#2021-1340). Primary human skin fibroblasts (NHDF-neo, Lonza; age and sex matched) were used as controls.

Measurement of cell size

For cell size quantification, 17,000 cells were seeded per dish (VWR, 150682) in regular culture medium and grown for 48 hours. Next, 4 μM CalceinAM dye (C3099, ThermoFisher Scientific) with 50 ng/mL Hoechst 33342 (14533, Sigma) in Live Cell Imaging Solution (A14291DJ, ThermoFisher Scientific) were added and cells were incubated for 15 minutes at 37 °C. Subsequently, cells were washed 2× with Live Cell Imaging Solution. Images were acquired using an Axio Observer Z1 microscope equipped with a 20×/0.8 objective and an AxioCam 712 mono (all from Zeiss). For imaging of calcein fluorescence, an EGFP HC filter set (AHF) was selected, and for visualization of Hoechst 33342 staining, a DAPI HC BrightLine Basic filter set (AHF) was applied. Quantification of data was performed using interactive measurement with ZEN 3.1 (Zeiss) and application of the modules "Measurement", "Image Analysis", and "Macro Environment". For recognition of nuclear staining (Hoechst 33342), Otsu Threshold (Light Regions) with a minimum area of 463 was used (the number of nuclei was determined). For measurement of the surface, Triangle Threshold (Light Regions) with a minimum area of 1000 was applied (determination of cell size). Finally, the area of cells was divided by the number of nuclei per image.

TFEB immunofluorescence

One day before experiments, 10,000 cells were seeded per dish (VWR, 150680) in regular culture medium and incubated overnight at 37 °C. Next, cells were washed 2× with DMEM ± aa and subsequently incubated for 1.5 hours at 37 °C. Next, cells were fixed with cold methanol (−20 °C)

for 10 minutes. After washing 3× with phosphate-buffered saline (PBS), samples were incubated for 7 minutes in 0.2% Triton X 100/PBS. Again, cells were washed 2× with PBS. Blocking was done in 5% goat serum (G9023, Sigma) in PBS. Next, anti-TFEB CL594 (CoraLite 594 conjugated TFEB antibody, CL594-13372, Proteintech; 1:200) was added in 1% bovine serum albumin (BSA)/PBS 200 μL/dish for 1.5 hours at room temperature. Subsequently, cells were washed 3× with 0.2% Triton/PBS for 10 minutes. Images were acquired using an Axio Observer Z1 microscope using a Plan-Apochromat 63×/1.4 oil objective (Zeiss) and filter set 31 (Zeiss). Quantification of mean fluorescence intensity was done with FIJI software in standardized areas of nuclei, cytoplasm, and background. After background correction, a ration of mean nuclear and mean cytoplasmic fluorescence was determined.

Immunoblotting

For experiments using whole-cell lysates, cells were cultured in T75 flasks for 4 to 6 days. Next, cells were washed 2× with DMEM ± aa and subsequently incubated in DMEM ± aa for 2 hours at 37 °C. Cells were harvested with TrypLE (Thermo Scientific), washed 3× in NaCl, and centrifuged a $300 \times g$ for 5 minutes at 4 °C. Pellets were lysed in 200 μL PhosphoSafe (TB402, Novagen) with protease and phosphatase inhibitors (P8340, P0044, both from Sigma, and Halt Protease Inhibitor #1860932, Thermo Scientific). Lysates were centrifuged for 5 minutes at $10,000 \times g$ at 4 °C.

For experiments with separation of nuclear and cytoplasmic fractions, cells were cultured in T75 flasks for 4 to 6 days. Subsequently, cells were incubated in DMEM ± aa for 1.5 hours at 37 °C. Cells were harvested with TrypLE (Thermo Scientific), washed 3× in NaCl, and centrifuged at $300 \times g$ for 5 minutes at 4 °C. Cellular fractions were obtained using the NE-PER Nuclear and Cytoplasmic Extraction Reagents kit (78835, Thermo Scientific) according to the manufacturer's protocol.

After removal of the supernatant, protein content was determined, and 20 μg of the samples were used. The supernatant was mixed with LDS sample buffer (NP0007, Novex by Invitrogen) and sample reducing agent (NP0004, Novex). Samples were loaded on 4% to 12% Bis-Tris gels (NP0321BOX, Invitrogen), and electrophoresis was performed using NuPage MOPS SDS Running Buffer (NP0001, Invitrogen). After electrophoresis, the gels were processed for western blotting and transferred to nitrocellulose membranes (#162-0146, BioRad) using NuPage transfer buffer (NP0006, Invitrogen). Blocking was done in 3% MP in TTBS. Only for TFEBpS211 blocking was done in 5% MP. The following primary antibodies were used: P-p70S6K (#9234; 1:1000; rabbit; Cell Signaling), p70S6K (#2708; 1:1000; rabbit; Cell Signaling), TFEBpS211 (#37681; 1:1000; rabbit; Cell Signaling), TFEB (13372-1-AP; 1:1000; rabbit; Proteintech, RRAGC (26989-1-AP; 1:1000; rabbit; Proteintech), Tubulin (T 9026; 1:1000; mouse; Sigma), Lamin AC (SAB4200236;

1:4000; mouse; Sigma). Incubation with primary antibodies for TFEBpS211/P-p70S6K/p70S6K was done in 5% BSA TTBS. All other antibodies were incubated in 3% MP in TTBS. The following secondary antibodies were used: anti-rabbit IgG horseradish peroxidase (HRP) (Amersham NA 934 V; 1:1000) and anti-mouse IgG HRP (Amersham NA 931 V; 1:1000). Incubation with secondary antibodies was done in 3% MP TTBS. BM Chemiluminescence blotting substrate (Roche) was used for visualization. Results were recorded using Chemidoc (BioRad). Bands were quantified using Image Lab software V 5.2.1 (BioRad). Statistical significance was assessed using t test.

For experiments using whole-cell lysates, results were related to the condition "control + aa." Values were normalized on tubulin.

For experiments with separation of nuclear and cytoplasmic fractions, results were related to the condition "control + aa." Values were normalized on tubulin (cytoplasm) or lamin AC (nucleus).

Structural modeling

AlphaFold Protein Structure Database (accession ID: Q9HB90; last accessed 04.09.2022, AlphaFold DB version 2022-06-01) was used to visualize RagC protein structure.[13]

Immunofluorescence of mTOR localization

Cells were detached and transferred to glass bottom dishes (Thermo 150680) and grown in regular culture medium (DMEM). For immunostaining, cells were washed with and subsequently cultured for 1.5 hours at 37 °C in DMEM medium with or without amino acids (for culture conditions, see section "Fibroblast culture"). Next, cells were fixed with 100% ethanol for 15 minutes. In the following, cells were washed 3× with PBS, and samples were blocked in 1% BSA in PBS for 1 hour at room temperature. CoraLite 594-conjugated mTOR monoclonal antibody (mouse IgG2a; Proteintech CL594-66888; 1:100) and anti-LAMP1 monoclonal antibody (mouse IgG1, abcam ab25630; 1:100) were used as primary antibodies. Samples were incubated for 1.5 hours in 1% BSA and subsequently washed 3× with PBS. For Lamp1 staining, Alexa Fluor 488 goat anti-mouse IgG1 (Invitrogen A21121; 1:1000) was used in 1% BSA in PBS for 30 minutes at room temperature in the dark. Fluorescence images were obtained using an Axio Observer Z1 microscope equipped with Apotome 3 and ZEN 3.5 pro software using a Plan-Apochromat 63×/1.4 oil objective and filter sets 38 HE and 63 HE (all from Zeiss).

Investigation of *RRAGC* variants in a HEK293 cell model

Prk5 Flag-RRAGB was a gift from Roberto Zoncu (Addgene plasmid #112755), and Prk5 HA-RRAGC was a gift

from David Sabatini and Kuang Shen (Addgene plasmid #99718). To create *RRAGC* vectors containing variants of interest, site-directed mutagenesis was performed using the Q5 site–directed mutagenesis kit (New England Biolabs). Sanger sequencing of vectors was performed to confirm the variants. HEK293 cells at 70% confluency were transfected with 1 µg of *RRAGB* and 1 µg of either wild-type or mutant *RRAGC* using Transit-X2 transfection reagent (MirusBio) in OptiMEM. Twenty-four hours after transfection, cells were incubated with either DMEM or DMEM Limiting Medium (Gibco) lacking both L-leucine and L-methionine. After 2 hours of incubation, cells were washed in PBS, collected, and lysed in NP-40 lysis buffer containing HALT protease and phosphatase inhibitors (ThermoFisher Scientific). Whole-cell lysate (20 µg) was denatured in LDS sample buffer and ran on a BOLT 4% to 12% Bis-Tris SDS PAGE Gel. After transfer to a polyvinylidene difluoride membrane, the membrane was blocked in 5% skimmed milk in PBS and incubated overnight in primary antibody. After 3 washes in PBS, the membrane was incubated with a secondary HRP antibody for 1 hour. After a further 3 washes in PBS, SuperSignal West Femto Maximum Sensitivity substrate was added to visualize the blot and imaged on a ChemiDoc MP Imaging system (BioRad). Bands were analyzed using ImageLab software (BioRad), and statistical analysis performed using Prism 9 software using intensity values obtained from 3 independent biological replicates.

All antibodies were from Cell Signaling Technology and used at a dilution of 1:1000 in 1% nonfat milk unless otherwise reported. Primary antibodies used were p70S6 kinase (#9202), phospho-S6 kinase (#9204), TFEB (#37785), and phospho-TFEB (Ser122) (#87932). A B-actin antibody (Ambion, 1:10,000) was used as a loading control on all blots. Secondary antibodies used include anti-Rabbit HRP (#7074, 1:5000) and anti-mouse HRP (DAKO, 1:10,000).

Results

Case reports

Individual #1 was the first child of healthy nonconsanguineous parents with European ancestry. The boy was born at 30^{+4} gestational weeks after normal pregnancy because of premature rupture of membranes (weight 1.75 kg [p71]/3.86 lb, lengths 47 cm [p96]/18.5 inches, head circumference 32 cm [p93]/12.6 inches). After birth, increasing lactate levels became evident (11 mmoL/L; norm < 1.6). Echocardiography demonstrated a large atrial septal defect of the secundum type and 2 small ventricular septal defects. During the following days, heart function deteriorated with global restrictive biventricular dysfunction (fractional shortening 15%-20%) and dilatation of the right atrium (Figure 1, Supplemental Videos 1 and 2). Lactate levels increased up to 22 mmoL/L, and ammonium

concentrations were elevated up to 670 µg/dL (norm < 228). Laboratory values indicated liver dysfunction (GOT 451 U/L, norm < 100; GPT 68 U/L, norm < 42; Ggt 230 U/L, norm < 181; quick 29%, norm > 64). Metabolic workup in urine revealed a strong elevation of Krebs-cycle intermediates, indicating mitochondrial dysfunction. Treatment with high-caloric infusion and application of detoxifying agents led to a normalization of ammonium levels. However, lactate concentrations remained high (25 mmoL/L). Brain magnetic resonance imaging revealed cavum septum pellucidum and pachygyria (Figure 1). The child died on the fourth day of life because of cardiocirculatory failure. Investigation of muscle tissue revealed no respiratory chain abnormalities. Brain autopsy confirmed pachygyria and additionally identified areas with polymicrogyria (Figure 1).

Individual #2 is the third child of nonconsanguineous parents of European ancestry. The boy was born after 40^{+6} weeks of gestation (weight 3.18 kg [p12]/7.01 lb, length 50 cm [p10]/19.7 inches, Apgar 4/9). Growth parameters were normal within the first 9 months (head circumference 43.5 cm [p41]/17.13 inches at age 6 months, height 70 cm [p32]/27.6 inches and weight 8.0 kg [p25]/17.64 lb at age 9 months). Motoric development was moderately delayed. At the age of 9 months, the boy was hospitalized because of acute cardiac failure. Echocardiography showed dilatation of the left ventricle with abnormal systolic and diastolic function. There was mild mitral, tricuspid, and pulmonary valve insufficiency. Brain magnetic resonance imaging showed abnormalities in the spectrum of septo-optic dysplasia (Figure 1). Eye examination revealed bilateral cataracts and optic nerve hypoplasia. The further clinical course was complicated by weight loss due to feeding difficulties and vomiting. Lactate levels increased up to 18 mmol/l. Additionally, severe liver dysfunction was present. Three weeks after clinical deterioration, the heart function further declined, and the boy died at the age of 10 months.

Individual #3 was the first child of healthy nonconsanguineous parents with European ancestry. The girl was born at 35^{+2} gestational weeks because of fetal hydrops and deterioration of cardiac function (weight 3.185 kg [p91]/7.02 lb, length 48 cm [p56]/18.9 inches, head circumference 33.5 cm [p67]/13.2 inches). Postnatal echocardiography revealed right ventricular enlargement and tricuspid valve insufficiency. Brain ultrasound demonstrated cavum septum pellucidum, as well as bilateral subependymal cysts in the caudothalamic groove (Figure 1). Moreover, signal intensity of the basal ganglia appeared increased. Eye examination revealed microspherophakia. Laboratory investigations showed increased lactate levels (max. 8.3 mmoL/L) and indicated liver dysfunction (GOT 129 U/L, norm < 100; Ggt 226 U/L, norm < 140; albumin 1.95 g/dL, norm > 2.8; quick 42%, norm > 70%). During further clinical course, the cardiac function of the child further deteriorated (severe DCM with systolic dysfunction, fractional shortening 11%). The girl died at the age of 1 month due to cardiac failure.
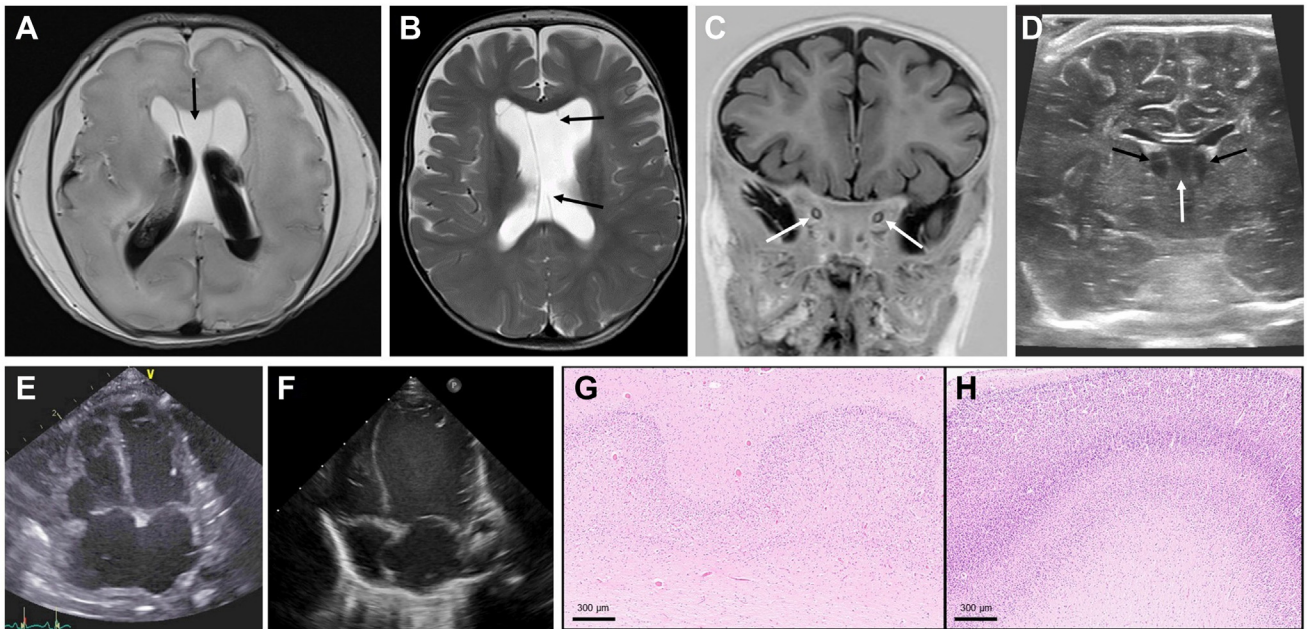
Figure 1   Clinical imaging and neuropathology in individuals with pathogenic variants in *RRAGC*. A. Brain MRI (T2-weighted, axial view) of individual #1 showing pachygyria, CSP (black arrow), and intraventricular hemorrhage due to coagulopathy caused by liver dysfunction. B. Brain MRI (T2-weighted, axial view) of individual #2 demonstrating CSP with partial aplasia of septal leaflets (black arrows). C. Brain MRI of individual #2 (T1-weighted, coronal view) showing bilateral hypoplasia of the optic nerves (white arrows). D. Brain ultrasound image of individual #3 demonstrating CSP (white arrow), as well as bilateral cystic structures in the caudothalamic groove (black arrows). Moreover, signal intensity of the basal ganglia appears increased. E. Echocardiographic image of individual #1 during the neonatal period, 4-chamber view, demonstrating severe DCM with globally impaired systolic function (fractional shortening 15%-20%; see also Supplemental Videos 1 and 2). F. Echocardiographic image of individual #3 during the neonatal period, 4-chamber view, showing severe DCM and systolic dysfunction (fractional shortening 11%). G. Histologic image (hematoxylin and eosin staining) from brain autopsy of individual #1 demonstrating focal polymicrogyria with a 4-layered cortex instead of the normal 6-layered isocortex (sample was acquired from the left temporal region). H. For comparison, a histologic image of a sample with normal 6-layered isocortex is depicted, which was derived from the occipital brain region of individual #1. CSP, cavum septum pellucidum; DCM, dilatative cardiomyopathy; MRI, magnetic resonance imaging.

Summarized clinical information is available in Supplemental Table 1.

Genetic findings

For all individuals, data analysis of trio-ES revealed no (likely) pathogenic variants in the context of an autosomal-recessive or mitochondrial inheritance pattern. A search for de novo variants revealed single-nucleotide variants in *RRAGC* in the 3 affected children: individual #1: *RRAGC*: NM_022157.4: c.269C>A; p.(Thr90Asn) (NC_000001.10:g.39322723G>T (GRCh37)/ NC_000001.11:g.38857051G>T (GRCh38)), CADD-score: 24.6 (calculated by https://cadd.gs.washington.edu/snv), coverage in exome 56-fold, variant allele frequency (VAF) of 38%; individual #2: NM_022157.4: c.353C>T; p.(Pro118Leu) (NC_000001.10:g.39322639G>A (GRCh37)/ NC_000001.11:g.38856967G>A (GRCh38)), CADD-score: 29.7, coverage in exome 83-fold, VAF of 53%; individual #3: NM_022157.4: c.343T>C; p.(Trp115Arg) (NC_000001. 10:g.39322649A>G (GRCh37)/NC_000001.11:g. 38856977A>G (GR Ch38)), CADD-score: 28.9, coverage in exome 228-fold, VAF of 52%. The variants were predicted to lead to amino acid substitutions at highly conserved positions in the nucleotide-binding region of RagC (Supplemental Figure 2). The variants identified in individuals #1 and #3 were not present in healthy controls either from the gnomAD database or in the Munich in-house database of approximately 25,000 exomes.[14] The variant identified in individual #2 (p.(Pro118Leu)) is present in 1 healthy control individual from the gnomAD database v.3.1.2, but manual visualization of sequencing data reveals a VAF of 0.25 to 0.3, indicating the presence of (somatic) mosaicism.

Although the VAF for the variants identified in individuals #1 to #3 by ES was not generally suspicious of mosaicism, Sanger sequencing was used to confirm the presence of the *RRAGC* variant in fibroblasts of individual #1, thus making a germline variant likely. Additional tissue samples for individuals #2 and #3 to confirm germline variant status were not available.

The *RRAGC* gene is considered to be intolerant for loss-of-function (LOF) variants as observed by metrics in the gnomAD database (pLI = 0.98, v.2.1.1).[13] However, multiple healthy individuals carrying LOF variants are present in gnomAD and the Munich in-house database. Thus,
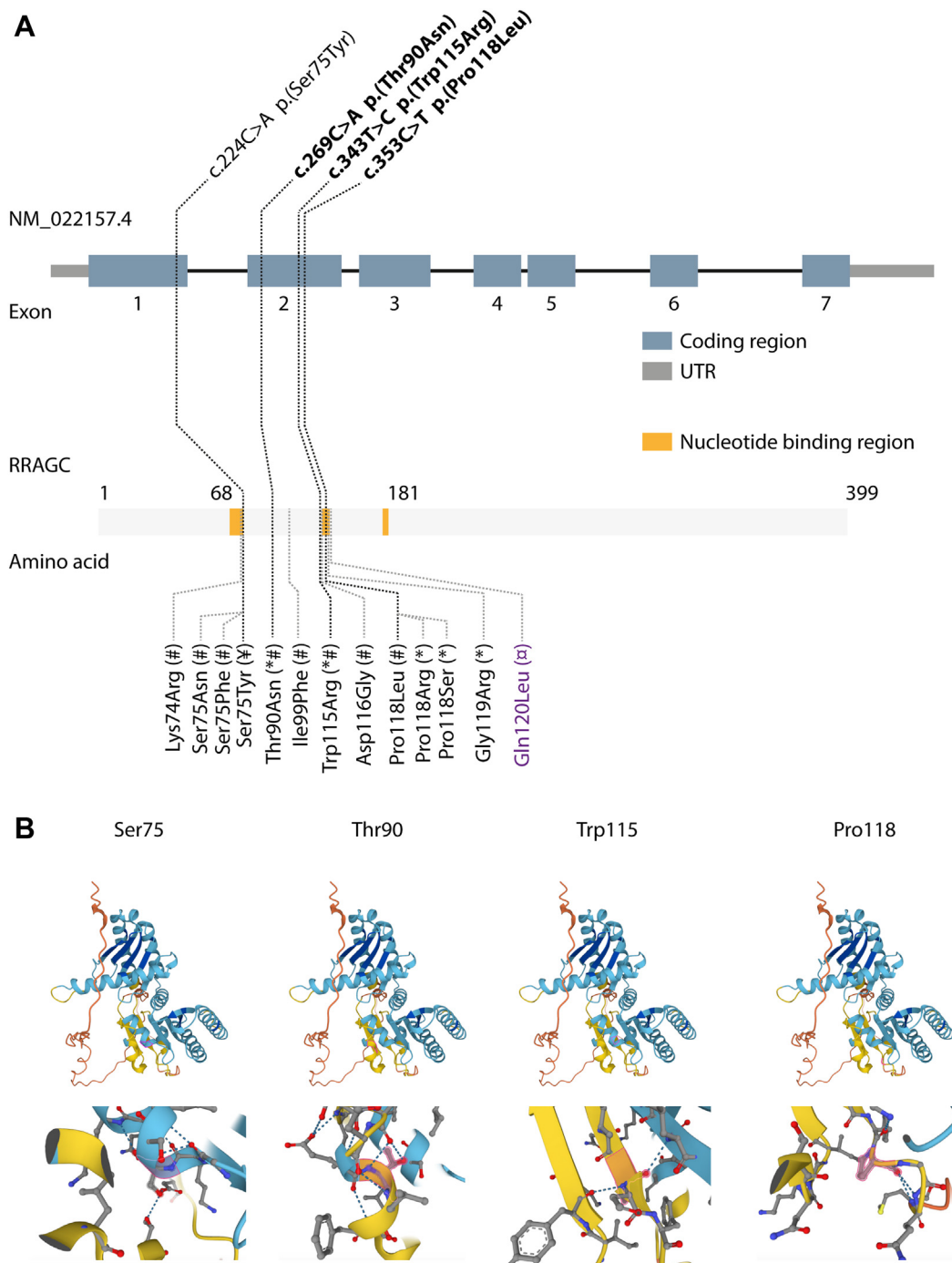
Figure 2 **Genetic findings in individuals with pathogenic variants in *RRAGC*.** A. Reported variants in *RRAGC* (NM_022157.4). The upper panel depicts the germline variants reported in affected individuals so far. Novel variants described in this report are described in bold. Intronic sequences are not to scale. Selected somatic variants reported in follicular lymphoma are described below the representation of the RagC protein. The 3 nucleotide-binding sites are depicted in yellow (residues 68-75, 116-120, 178-181). Respective publications are annotated in round brackets as follows: #;[15] *;[16] ¤;[17] ¥.[12] Of those COSMIC variants, the variants in black are suspected to lead to an enhanced binding of GDP, subsequently leading to mTORC1 activation. The variant Gln120Leu is suspected to lead to an increased binding of GTP, thus leading to decreased mTORC1 activation. B. Protein model of RagC obtained from AlphaFold, colors according to AlphaFold per-residue confidence score (pLDDT) between 0 and 100 (dark blue: very confident, pLDDT > 90; light blue: confident, pLDDT: 70-90; yellow: low, pLDDT: 70-50; red: very low, pLDDT: < 50).[13] The position of amino acid affected by missense variants in *RRAGC* from our study (Thr90, Trp115, Pro118; panels B-D) and by Long et al (Ser75, panel A) are highlighted in magenta.[8] Lower panels show zooms of the respective regions. Overall, the respective residues affect the nucleotide sensing elements of the RagC protein. mTORC1, mechanistic target of rapamycin complex 1.
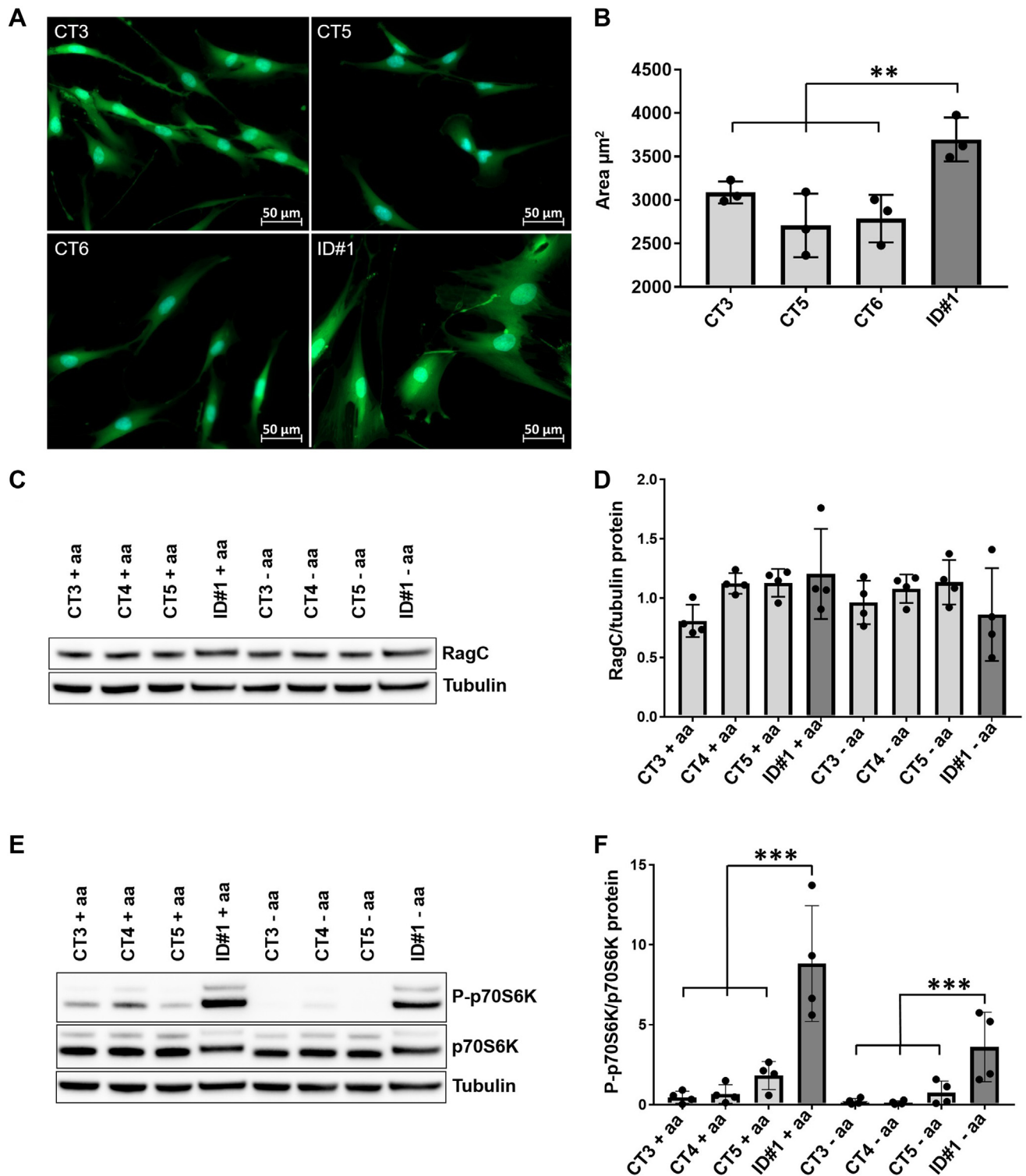
Figure 3   The pathogenic p.(Thr90Asn) variant in *RRAGC* is associated with increased cell size and dysregulates p70S6K signaling. A, B. Determination of cell size. A. Representative microscope images of 3 age- and sex-matched control fibroblast lines (CT3, CT5, CT6) and affected individual ID #1. B. Quantitative analysis of cell size. Bar graphs depict the results of 3 independent experiments (number of individual cells analyzed: CT3 = 1070; CT5 = 867; CT6 = 1053; ID #1 = 829). C. Representative immunoblot images of RagC protein levels in control (CT3, CT4, CT5) and patient-derived (ID#1) fibroblasts. Depicted are conditions with or without amino acid supplementation (+aa/−aa). Tubulin served as a loading marker. D. Quantitated density of RagC western blot bands from 3 independent biological replicates. E. Representative immunoblot images of p70S6K and phosphorylated p70S6K (P-p70S6K) under conditions with or without amino acid supplementation (+aa/−aa). Tubulin served as a loading marker. F. Quantitated density of RagC western blot bands from 3 independent biological replicates. Bands were quantified using ImageJ software. Statistical significance was assessed using *t* test. For all of the above results, average values are presented as the mean ± SD; **$*P < .01$ and ***$P < .001$ significantly different from controls. aa, amino acid.

RRAGC haploinsufficiency as an underlying disease mechanism was considered unlikely. Additionally, the gene also shows a constraint against missense variants (Z = 2.46; gnomAD v.2.1.1).[14] When closely investigating the identified missense variants in individuals #1 (p.(Thr90Asn)), #2 (p.(Pro118Leu)), and #3 (p.(Trp115Arg)), as well as the previously described missense variant p.(Ser75Tyr) (Figure 2), it became apparent that all 4 variants had previously been reported in the COSMIC database and had been implicated in constitutional Rag heterodimer activation in the context of follicular lymphoma, leading to the hypothesis that the identified *RRAGC* variants in the individuals may act via increased mTORC1 activation.[18-20]

Of note, 1 additional individual carrying the de novo variant p.(Trp115Arg) in *RRAGC* was reported in a cohort study of individuals with developmental disorders. However, no clinical details were provided in the study. We tried to obtain phenotypic data but were only able to retrieve the information that the individual had cardiomyopathy.[21]

Structural modeling

A protein model of RagC was obtained from AlphaFold to visualize the location of the amino acid changes caused by the missense variants p.(Thr90Asn), p.(Trp115Arg), p.(Pro118Leu), and p.(Ser75Tyr). The analysis indicates that all variants affect amino acid residues close to the nucleotide sensing elements of the RagC protein (Figure 2B).

The p.(Thr90Asn) variant in *RRAGC* is associated with increased cell size

The activity of the mTORC1 pathway is essential for cell growth. Overactivation of mTORC1 has been shown to increase cell size.[9] Accordingly, we investigated cell size in patient-derived fibroblasts. Experiments revealed that fibroblasts of individual #1 were significantly larger compared with healthy age- and sex-matched controls (Figure 3A and B).

Fibroblasts carrying the p.(Thr90Asn) variant show disturbed p70S6K signaling

Immunoblotting of RagC protein levels revealed no differences between control fibroblasts and fibroblasts derived from individual #1 under ± aa culture conditions (Figure 3C and D). Next, we analyzed a potential effect of the p.(Thr90Asn) variant on p70S6K (ribosomal protein S6 kinase 1), which is a major target of the mTORC1 pathway. Under physiological conditions, presence of amino acids triggers phosphorylation and activation of p70S6K.[2] Amino acid withdrawal leads to inactivation of this pathway. To investigate alterations in amino acid dependence of mTORC/p70S6K signaling, we performed immunoblotting experiments under ± aa culture conditions. The levels of phosphorylated p70S6K were significantly higher in patient compared with control fibroblasts. In controls, amino acid starvation led to a decrease of p70S6K phosphorylation, whereas in patient-derived cells, there was less difference between culture conditions, and p70S6K phosphorylation remained high (Figure 3E and F). Together, these results show hyperactivated p70S6K signaling in both amino acid–enriched and –depleted circumstances in patient fibroblasts, suggesting mTORC1 hyperactivity.

TFEB levels are decreased and subcellular localization is altered in fibroblasts carrying the p.(Thr90Asn) variant

TFEB subcellular distribution is dependent upon RagC.[4] In a state of mTORC1 activation, TFEB is retained in the cytosol, whereas mTORC1 inactivation leads to a predominantly nuclear localization.[20] To investigate a potential dysregulation of TFEB activity, we performed immunoblotting. Strikingly, levels of total TFEB were reduced in patient cells (Figure 4A). In contrast, phosphorylated TFEB was significantly increased in patient cells consistent with an overactivation of mTORC1 (Figure 4A and B). The physiological reduction of TFEB phosphorylation in response to amino acid starvation was impaired. Next, we investigated the subcellular localization of TFEB by immunofluorescence microscopy. Although TFEB was shifted to the nucleus in the absence of amino acids in control cells, TFEB was mainly retained in the cytoplasm in patient cells (Figure 4C). The impaired shift of TFEB into the nucleus was also confirmed by immunoblotting of nuclear and cytoplasmic fractions (Figure 4D and E).

In fibroblasts carrying the p.(Thr90Asn) variant, mTOR remains localized on the lysosome despite amino acid starvation

To investigate mTOR localization during different culture conditions, cells were stained with antibodies against mTOR and lysosomal-associated membrane protein 1 (Lamp1). As depicted in Figure 5A, during the presence of amino acids, mTOR was mainly localized at the lysosomes in patient and control fibroblasts. However, during amino acid starvation, mTOR redistributed to the cytosol in control fibroblasts. In contrast, mTOR remained mainly at the lysosomes in patient-derived fibroblasts. These findings suggest that the p.(Thr90Asn) variant decouples mTOR activation from cellular nutritional state. Interestingly, the amount of lysosomes was not clearly reduced in patient-derived cells (by visual inspection). This might indicate that compensatory mechanisms help to maintain lysosomal biogenesis despite mTOR pathway hyperactivation. Additional microscopy images are shown in Supplemental Figure 3.
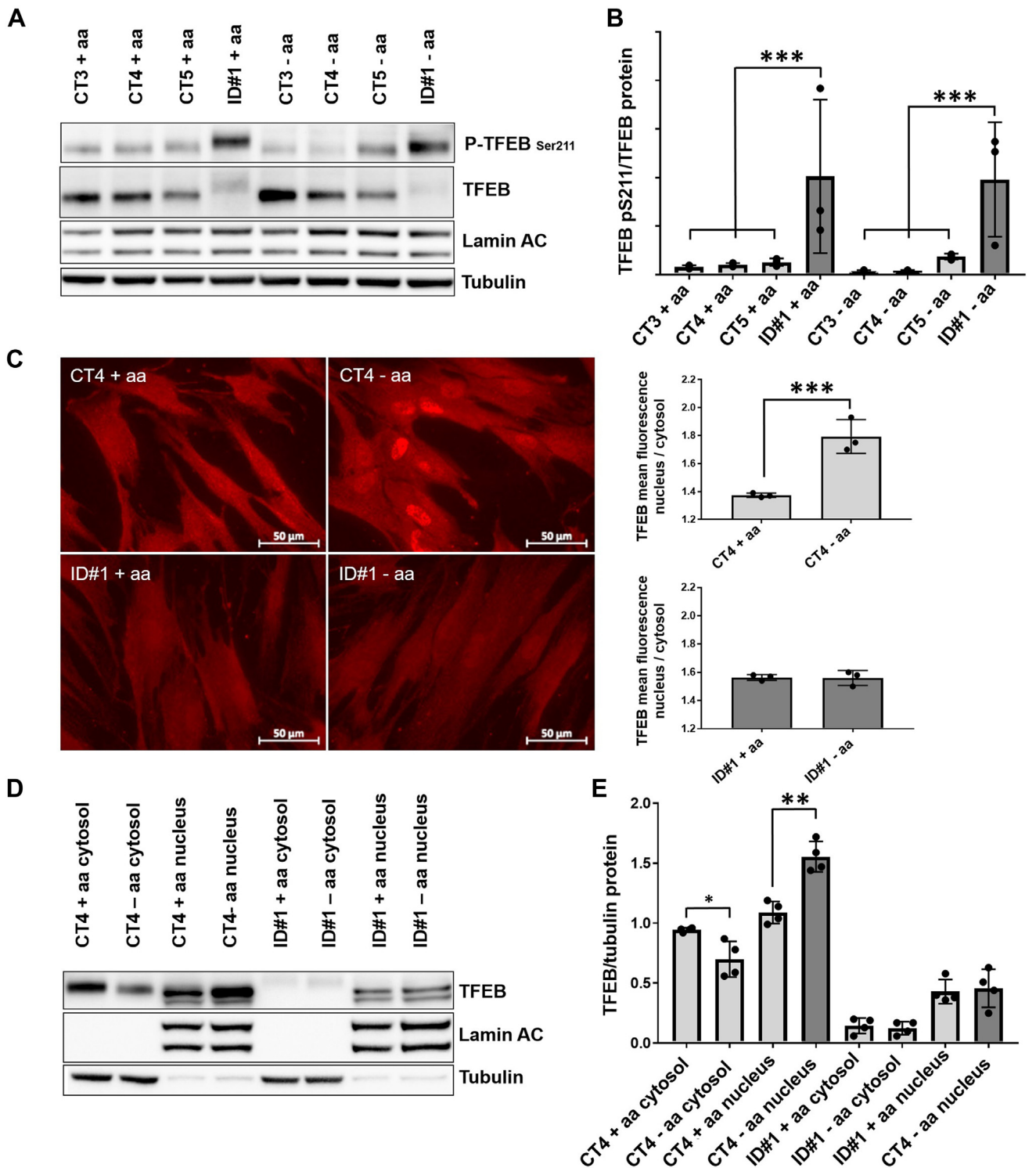
Figure 4   The pathogenic p.(Thr90Asn) variant in *RRAGC* disrupts TFEB signaling. A. Representative immunoblot images of TFEB and phosphorylated TFEB (P-TFEB$_{Ser211}$). Depicted are control (CT3, CT4, CT5) and patient-derived (ID#1) fibroblasts under conditions with or without amino acid supplementation (+aa/−aa). Lamin AC and tubulin served as loading markers. B. Quantitated density of TFEB and P-TFEBSer211 western blot bands of 3 independent biological replicates. C. Left panels: representative microscope images of TFEB immunofluorescence in control (CT4) and patient (ID #1) fibroblasts under conditions with or without amino acid supplementation (+aa/ −aa). Right panel: quantitative analysis of TFEB immunofluorescence images. Bar graphs represent results from 3 independent experiments (number of individual cells analyzed: CT4 + aa = 158; CT4 − aa = 150; ID #1 + aa = 177; ID #1 − aa = 206). D. Representative immunoblot images of TFEB in nuclear and cytosolic fractions under conditions with or without amino acid supplementation (+aa/−aa). E. Quantitated density of TFEB western blot bands from 4 independent biological replicates. Bands were quantified using ImageJ software. Statistical significance was assessed using *t* test. For all of the above results, average values are presented as the mean ± SD; *$P < .05$, **$P < .01$, and ***$P < .001$ significantly different from controls. aa, amino acid; TFEB, transcription factor EB.

Pathogenicity of *RRAGC* variants is confirmed in a HEK293 cell model

To determine the effect of each variant identified in this study on the mTOR signaling pathway, recombinant wild-type or mutant *RRAGC* (p.(Thr90Asn), p.(Trp115Arg), and p.(Pro118Leu)) was co-expressed with recombinant wild-type *RRAGB* in HEK293 cells. A vector containing the previously published *RRAGC* variant p.(Ser75Tyr) was used as a positive control. Immunoblotting of whole-cell lysate after amino acid starvation revealed increased p70S6K phosphorylation for all pathogenic variants identified in keeping with activation of the mTOR pathway. In addition, increased TFEB phosphorylation was observed in cells transfected with mutant *RRAGC* ([Figure 5](#)A-C). These results confirm that all of the investigated *RRAGC* variants induce aberrant mTOR signaling.

Discussion

The amino acid–dependent regulation of mTORC1 is an essential pathway that orchestrates de novo protein synthesis and cell growth in response to metabolic cues.[22] In the brain, mTOR signaling has been linked to key aspects of central nervous system development, such as neuronal differentiation and synaptic plasticity.[23] In the heart, mTOR signaling is known to contribute to embryonic cardiovascular development and postnatal maintenance of cardiac function.[15]

Hyperactivated mTOR signaling has been described to cause a variety of neurodevelopmental syndromes, so-called mTORopathies, with structural brain malformations, such as focal cortical dysplasia and hemimegalencephaly.[16,17] Of note, these diseases may be caused by germline variants, as well as by mosaic variants with variable tissue distribution.[24] Clinical features of mTORopathies include profound developmental delay, behavioral abnormalities, and epilepsy. It was suggested that the severity of the clinical phenotype depends on the underlying variant and the degree of mTOR activation, as well as the mosaic tissue distribution.[24]

The list of known disease genes affecting mTOR signaling already includes the Rag family members *RRAGA* and *RRAGD*, which are associated with cataracts, nephropathy, and dilated cardiomyopathy.[6,7] For *RRAGC*, recurrent, activating somatic variants, including the variants p.(Ser75Tyr), p.(Thr90Asn), p.(Pro118Leu), and p.(Trp115Arg), have been reported in follicular lymphoma ([Figure 1](#)).[19,20] The crystal structure of the nucleotide-binding site of RagC and respective RagC variants has been thoroughly investigated.[25] It was observed that specific oncogenic variants in *RRAGC* led to increased GDP binding by variant-specific structural changes of RagC. In 2016, an *RRAGC* germline variant in a child with lethal syndromic cardiomyopathy was described, suggesting that *RRAGC* might be another candidate disease gene within the expanding field of mTORopathies.[8] In addition, an individual carrying the de novo variant p.(Trp115Arg) in *RRAGC* was reported in a large cohort study of individuals with developmental disorders.[21] However, apart from the information that the individual had cardiomyopathy, no phenotypic details of this individual were available.

Our report on 3 additional individuals with pathogenic mTOR-activating *RRAGC* variants establishes disturbed RagC signaling as cause of a severe early-onset disease with multiple system involvement and lethal DCM as a core clinical feature. We expand the clinical spectrum with organ affections including brain (structural abnormalities, cortical dysplasia), liver (hepatic dysfunction), and eyes (cataracts, microspherophakia). Moreover, we describe metabolic abnormalities with lactic acidosis and hyperammonemia, which might be caused by a combination of secondary mitochondrial dysfunction and organ failure. As observed in individuals #1 and #3, *RRAGC* variants may even cause acute neonatal deterioration. This is in line with studies in mice demonstrating that constitutive RagA activity leads to energetic exhaustion and accelerated neonatal death.[22]

Interestingly, the importance of mTOR pathway hyperactivation for malformations of cortical development was recently described for NPRL3 loss, a component of the GATOR1 complex.[26] Focal Nprl3 knockout in fetal mouse cortex caused disturbed cytoarchitecture with altered cortical lamination and white matter heterotopia. This finding is in line with the brain pathology observed in individual #1.

The severe disease phenotypes observed in the individuals reported here seem to be the consequence of a germline variant with strong mTOR activation. As shown by our experiments in patient-derived fibroblasts, the p.(Thr90Asn) variant leads to increased cell size, hyperactivated p70S6K signaling, and disturbed subcellular TFEB distribution. Additional studies using a HEK293 cell model confirmed these findings for the p.(Trp115Arg) and p.(Pro118Leu) variants.

So far, treatment for mTORopathies faces many difficulties and is not available for the majority of subforms. Current research focuses on rapamycin and related drugs (sirolimus, everolimus) to inhibit mTOR activity.[27,28] A prime example for the effectiveness of this approach is the application of everolimus in patients with tuberous sclerosis with subependymal giant cell astrocytomas.[27] Moreover, mTORC1 blockade reduced cardiac derangements in mouse models induced by genetic and metabolic disorders and has been reported to extend life span in mice.[28] Therefore, it has been suggested that pharmacologic inhibition of mTOR may represent a therapeutic strategy to confer cardioprotection.

However, in contrast to the above findings, Kim et al[9] observed that inhibition of mTOR activity in a zebrafish model of the *RRAGC* p.(Ser75Tyr) variant was not effective. Instead, TFEB overexpression rescued the cardiomyopathy phenotype. This controversy underlines that currently no recommendation for treatment of individuals with pathogenic *RRAGC* variants can be given. Of note, in a recent
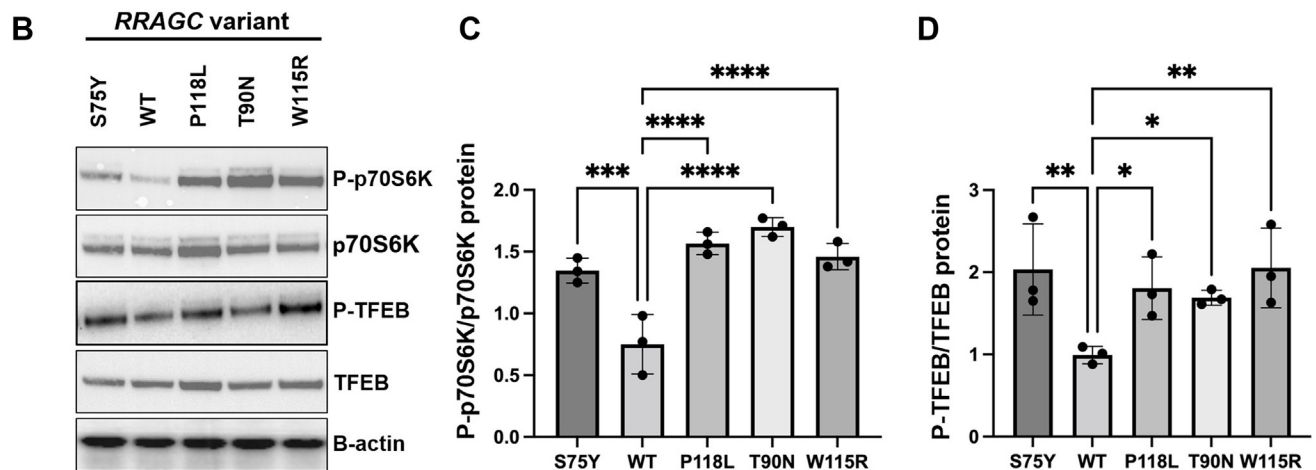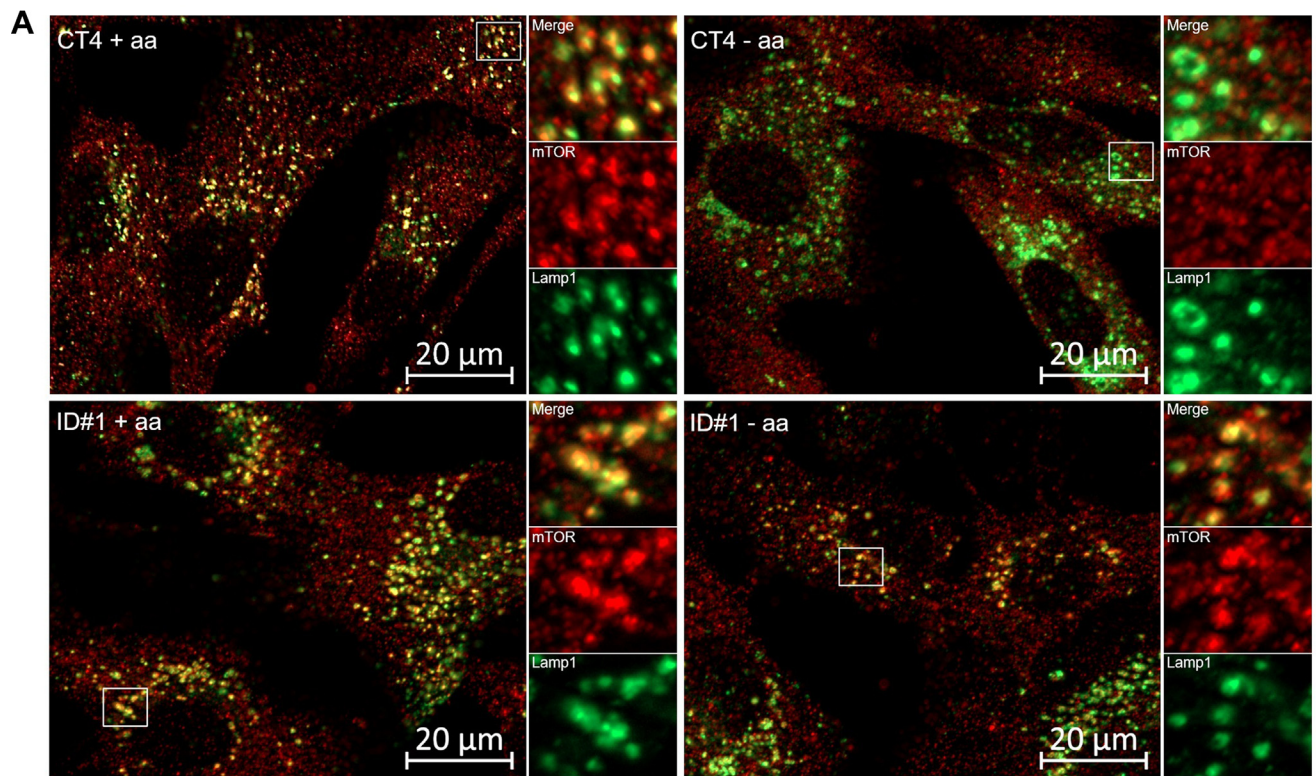
Figure 5   Subcellular localization of mTOR and biochemical analysis of published and novel variants in *RRAGC*. A. Patient (ID #1) and control (CT4) fibroblasts were stained with antibodies against mTOR and lysosomal-associated membrane protein 1 (Lamp1). Cells were cultured in the presence (+aa) or absence (−aa) of amino acids. Images show representative findings from 3 independent experiments. During the presence of amino acids, mTOR is mainly localized at the lysosomes. No clear differences between patient and control fibroblasts are visible under this condition. However, during amino acid starvation, mTOR redistributes to the cytosol in control fibroblasts. In contrast, mTOR remains mainly localized at the lysosomes in patient-derived fibroblasts. These findings suggest that the p.(Thr90Asn) variant decouples mTOR activation from nutritional state. B. Representative western blot of protein lysates from HEK293 cells transfected with wild-type or mutant *RRAGC* incubated in media lacking L-leucine and L-methionine for 90 minutes. Whole-cell lysates were assessed for phosphorylated and total p70S6K and TFEB. B-actin was used as a loading control. The effect of the previously published variant p.(Ser75Tyr) was also assessed as a positive control. All novel variants were found to significantly increase S6 kinase and TFEB phosphorylation compared with the wild type. C, D. Quantification of (C) phosphorylated relative to total p70S6K and (D) phosphorylated TFEB relative to total TFEB based on 3 independent biological replicates. Average values are presented as the mean ± SD. Significance was calculated using an ordinary one-way ANOVA in PRISM 9. $*P < .05$, $**P < .01$, $***P < .001$, $****P < .0001$. aa, amino acid; ANOVA, analysis of variance; mTOR, mechanistic target of rapamycin; TFEB, transcription factor EB.

publication, it was shown that TFEB phosphorylation by mTORC1 is specifically regulated through a RagC-dependent mechanism (lysosomal mTORC1–TFEB–Rag–Ragulator megacomplex).[29] The authors postulate that modulation of TFEB phosphorylation might be relevant for treatment of various human diseases. In this context, it is of interest that several drugs are known that are able to increase and or activate TFEB (eg, siramesine, quercetin, digoxin, ikarugamycin, and alexidine dihydrochloride).[30-32] Future studies will be required to investigate in how far these drugs could play a role in the treatment of RagC-related disease.

In summary, our work establishes variants in *RRAGC*, affecting mTORC1- and TFEB signaling, as cause of a severe mTORopathy with unfavorable prognosis.

Data Availability

Sequence data sets have been generated and contributed by different study sites and have not been deposited in a public repository because of varying local consent regulations. Depersonalized data and additional experimental data that this study is based on can be provided upon request.

Acknowledgments

Funding

Author Information

Conceptualization: M.R.F.R., F.D., J.A.P.; Data Curation: M.R.F.R., M.B., A.S., A.M.S.R., I.M.C., O.K., J.H., D.P., T.B., E.G., K.M.; Formal Analysis: A.S., A.M.S.R., I.M.C., F.D., J.A.P., E.G., K.M.; Funding Acquisition: F.D., J.A.P., M.R.F.R.; Investigation: A.S., T.O., K.L., R.J.T.R., M.B., L.A., A.M.S.R., I.M.C., I.J.C.L., D.H., D.K., R.B., M.S., A.P.A.S.; Resources: E.M., F.D., J.A.P., R.R.; Supervision: F.D.; Visualization: M.B., A.S., J.A.P., F.D., D.P., D.K., R.B.; Writing-original draft: M.R.F.R., F.D., J.A.P., M.B.; Writing-review and editing: M.R.F.R., F.D., J.A.P., M.B., R.R., D.W., E.M., E.N.-J., R.J.T.R., T.B., L.A.

Ethics Declaration

Written informed consent was obtained from the legal guardians of the individuals investigated in this study. The work was carried out in accordance with the regulations of the institutional review boards (Heinrich-Heine-University Düsseldorf, University Hospital Münster, and Maastricht University Medical Center). The use of patient-derived cells for research purposes was approved by the ethical committee of the Heinrich-Heine-University Düsseldorf (#2021-1340)

Conflict of Interest

The authors declare no conflicts of interest.

Additional Information

The online version of this article (https://doi.org/10.1016/j.gim.2023.100838) contains supplementary material, which is available to authorized users.

Affiliations

[1]Department of Clinical Genetics, Maastricht University Medical Center, Maastricht, The Netherlands; [2]Department of General Pediatrics, Neonatology and Pediatric Cardiology, Medical Faculty, Heinrich-Heine-University, Düsseldorf, Germany; [3]Institute of Human Genetics, Klinikum rechts der Isar, School of Medicine, Technical University of Munich, Munich, Germany; [4]Department of Human Genetics, Radboud University Medical Center, Nijmegen, The Netherlands; [5]University Children's Hospital, University Hospital Muenster, Münster, Germany; [6]Institute for Human Genetics, University Hospital Muenster, Muenster, Germany; [7]Leeds Institute of Medical Research, University of Leeds, Leeds, United Kingdom; [8]Department of Paediatric Neurology and Developmental Medicine, Hauner Children's Hospital, Ludwig Maximilian University of Munich, Munich, Germany; [9]Institute of Neuropathology, Medical Faculty, Heinrich-Heine-

University, Düsseldorf, Germany; [10]Translational Metabolic Laboratory, Department of Pediatrics, Radboud University Medical Center, Nijmegen, The Netherlands; [11]Institute of Human Genetics, Medical Faculty, Heinrich-Heine-University, Düsseldorf, Germany; [12]Department of Diagnostic and Interventional Radiology, University Hospital, Düsseldorf, Germany; [13]Department of Paediatrics, Maastricht University Medical Center, Maastricht, The Netherlands

References

1. Sancak Y, Sabatini DM. Rag proteins regulate amino-acid-induced mTORC1 signalling. *Biochem Soc Trans*. 2009;37(1):289-290. http://doi.org/10.1042/BST0370289

2. Sancak Y, Peterson TR, Shaul YD, et al. The Rag GTPases bind raptor and mediate amino acid signaling to mTORC1. *Science*. 2008;320(5882):1496-1501. http://doi.org/10.1126/science.1157535

3. Napolitano G, Di Malta C, Esposito A, et al. A substrate-specific mTORC1 pathway underlies Birt-Hogg-Dube syndrome. *Nature*. 2020;585(7826):597-602. http://doi.org/10.1038/s41586-020-2444-0

4. Sardiello M, Palmieri M, di Ronza A, et al. A gene network regulating lysosomal biogenesis and function. *Science*. 2009;325(5939):473-477. http://doi.org/10.1126/science.1174447

5. Hartman NW, Lin TV, Zhang L, Paquelet GE, Feliciano DM, Bordey A. mTORC1 targets the translational repressor 4E-BP 2, but not S6 kinase 1/2, to regulate neural stem cell self-renewal in vivo. *Cell Rep*. 2013;5(2):433-444. http://doi.org/10.1016/j.celrep.2013.09.017

6. Chen JH, Huang C, Zhang B, et al. Mutations of RagA GTPase in mTORC1 pathway are associated with autosomal dominant cataracts. *PLoS Genet*. 2016;12(6):e1006090. http://doi.org/10.1371/journal.pgen.1006090

7. Schlingmann KP, Jouret F, Shen K, et al. mTOR-activating mutations in RRAGD are causative for kidney tubulopathy and cardiomyopathy. *J Am Soc Nephrol*. 2021;32(11):2885-2899. http://doi.org/10.1681/ASN.2021030333

8. Long PA, Zimmermann MT, Kim M, Evans JM, Xu X, Olson TM. De novo RRAGC mutation activates mTORC1 signaling in syndromic fetal dilated cardiomyopathy. *Hum Genet*. 2016;135(8):909-917. http://doi.org/10.1007/s00439-016-1685-3

9. Kim M, Lu L, Dvornikov AV, et al. TFEB overexpression, not mTOR inhibition, ameliorates RagC(S75Y) cardiomyopathy. *Int J Mol Sci*. 2021;22(11):5494. http://doi.org/10.3390/ijms22115494

10. Brunet T, Jech R, Brugger M, et al. De novo variants in neurodevelopmental disorders-experiences from a tertiary care center. *Clin Genet*. 2021;100(1):14-28. http://doi.org/10.1111/cge.13946

11. Sobreira N, Schiettecatte F, Valle D, Hamosh A. GeneMatcher: a matching tool for connecting investigators with an interest in the same gene. *Hum Mutat*. 2015;36(10):928-930. http://doi.org/10.1002/humu.22844

12. Richards S, Aziz N, Bale S, et al. Standards and guidelines for the interpretation of sequence variants: a joint consensus recommendation of the American College of Medical Genetics and Genomics and the Association for Molecular Pathology. *Genet Med*. 2015;17(5):405-424. http://doi.org/10.1038/gim.2015.30

13. Jumper J, Evans R, Pritzel A, et al. Highly accurate protein structure prediction with AlphaFold. *Nature*. 2021;596(7873):583-589. http://doi.org/10.1038/s41586-021-03819-2

14. Karczewski KJ, Francioli LC, Tiao G, et al. The mutational constraint spectrum quantified from variation in 141,456 humans. *Nature*. 2020;581(7809):434-443. http://doi.org/10.1038/s41586-020-2308-7

15. Sciarretta S, Volpe M, Sadoshima J. Mammalian target of rapamycin signaling in cardiac physiology and disease. *Circ Res*. 2014;114(3):549-564. http://doi.org/10.1161/CIRCRESAHA.114.302022

16. Reijnders MRF, Kousi M, van Woerden GM, et al. Variation in a range of mTOR-related genes associates with intracranial volume and intellectual disability. *Nat Commun*. 2017;8(1):1052. http://doi.org/10.1038/s41467-017-00933-6

17. Mirzaa GM, Campbell CD, Solovieff N, et al. Association of MTOR mutations with developmental brain disorders, including megalencephaly, focal cortical dysplasia, and pigmentary mosaicism. *JAMA Neurol*. 2016;73(7):836-845. http://doi.org/10.1001/jamaneurol.2016.0363

18. Tate JG, Bamford S, Jubb HC, et al. COSMIC: the catalogue of somatic mutations in cancer. *Nucleic Acids Res*. 2019;47(D1):D941-D947. http://doi.org/10.1093/nar/gky1015

19. Okosun J, Wolfson RL, Wang J, et al. Recurrent mTORC1-activating RRAGC mutations in follicular lymphoma. *Nat Genet*. 2016;48(2):183-188. http://doi.org/10.1038/ng.3473

20. Ying ZX, Jin M, Peterson LF, et al. Recurrent mutations in the MTOR regulator RRAGC in follicular lymphoma. *Clin Cancer Res*. 2016;22(21):5383-5393. http://doi.org/10.1158/1078-0432.CCR-16-0609

21. Kaplanis J, Samocha KE, Wiel L, et al. Evidence for 28 genetic disorders discovered by combining healthcare and research data. *Nature*. 2020;586(7831):757-762. http://doi.org/10.1038/s41586-020-2832-5

22. Efeyan A, Zoncu R, Chang S, et al. Regulation of mTORC1 by the Rag GTPases is necessary for neonatal autophagy and survival. *Nature*. 2013;493(7434):679-683. http://doi.org/10.1038/nature11745

23. Switon K, Kotulska K, Janusz-Kaminska A, Zmorzynska J, Jaworski J. Molecular neurobiology of mTOR. *Neuroscience*. 2017;341:112-153. http://doi.org/10.1016/j.neuroscience.2016.11.017

24. Dobyns WB, Mirzaa GM. Megalencephaly syndromes associated with mutations of core components of the PI3K-AKT-MTOR pathway: PIK3CA, PIK3R2, AKT3, and MTOR. *Am J Med Genet C Semin Med Genet*. 2019;181(4):582-590. http://doi.org/10.1002/ajmg.c.31736

25. Anandapadamanaban M, Masson GR, Perisic O, et al. Architecture of human Rag GTPase heterodimers and their complex with mTORC1. *Science*. 2019;366(6462):203-210. http://doi.org/10.1126/science.aax3939

26. Iffland PH, Everett ME, Cobb-Pitstick KM, et al. NPRL3 loss alters neuronal morphology, mTOR localization, cortical lamination and seizure threshold. *Brain*. 2022;145(11):3872-3885. http://doi.org/10.1093/brain/awac044

27. Karalis V, Bateup HS. Current approaches and future directions for the treatment of mTORopathies. *Dev Neurosci*. 2021;43(3-4):143-158. http://doi.org/10.1159/000515672

28. Sciarretta S, Forte M, Frati G, Sadoshima J. New insights into the role of mTOR signaling in the cardiovascular system. *Circ Res*. 2018;122(3):489-505. http://doi.org/10.1161/CIRCRESAHA.117.311147

29. Cui Z, Napolitano G, de Araujo MEG, et al. Structure of the lysosomal mTORC1–TFEB–Rag–Ragulator megacomplex. *Nature*. 2023;614(7948):572-579. http://doi.org/10.1038/s41586-022-05652-7

30. Wang C, Niederstrasser H, Douglas PM, et al. Small-molecule TFEB pathway agonists that ameliorate metabolic syndrome in mice and extend *C elegans* lifespan. *Nat Commun*. 2017;8(1):2270. http://doi.org/10.1038/s41467-017-02332-3

31. Huang Y, Chen Y, Shaw AM, Goldfine H, Tian J, Cai J. Enhancing TFEB-mediated cellular degradation pathways by the mTORC1 inhibitor quercetin. *Oxid Med Cell Longev*. 2018;2018:5073420. http://doi.org/10.1155/2018/5073420

32. Zhitomirsky B, Yunaev A, Kreiserman R, Kaplan A, Stark M, Assaraf YG. Lysosomotropic drugs activate TFEB via lysosomal membrane fluidization and consequent inhibition of mTORC1 activity. *Cell Death Dis*. 2018;9(12):1191. http://doi.org/10.1038/s41419-018-1227-0